Precise Localization of Mobile Robots in GNSS-Challenged Urban Mobility Scenarios: Experimental Insights on the Influence of Anchor Vertical Placement Using Ultra-Wideband

Bhavinkumar Patel[1], Ellahe Khosravi[1], Mohammed Obaid[1], Prof. Dr. Henner Gärtner[1]

[1] Faculty of Sustainable Engineering, Hamburg University of Applied Sciences (HAW Hamburg), Germany

Abstract **Autonomous navigation of mobile robots and micromobility vehicles in dense urban corridors requires decimeter-level localization accuracy that GNSS (Global Navigation Satellite System) alone cannot reliably provide. Ultra-wideband (UWB) offers a promising complementary solution via precise time-of-flight measurements. However, UWB outdoor localization remains underexplored, particularly how anchor geometry affects positioning performance. This paper presents experimental insights into the influence of anchor vertical placement on two-dimensional (2D) UWB positioning accuracy outdoors. Three anchor-height configurations were evaluated over a 7 m x 10 m field using a custom Qorvo DWM3000-based UWB beacon system built at HAW Hamburg: one homogeneous baseline configuration (all anchors at 2.7 m) and two configurations with incremental height variations up to 0.6 m. Static measurements were conducted with the tag mounted at 0.80 m to simulate a mobile robot. Positioning performance was assessed via mean position offsets, standard deviations, 2D positional scatter, and Dilution of Precision (DOP) analysis.**

Keywords— Ultra-wideband, UWB outdoor localization, UWB outdoor positioning, Qorvo DWM3000, anchor vertical placement, anchor geometry, dilution of precision, mobile robots, micromobility vehicles, GNSS-challenged environments

I. INTRODUCTION

The increasing deployment of autonomous mobile robots and micromobility vehicles in urban environments demands robust, decimeter-level positioning capabilities. Classical satellite-based navigation using the Global Navigation Satellite System (GNSS) is widely available but fails to meet precision and reliability requirements in dense urban corridors, under bridges, in tunnels, and wherever signal multipath or blockage degrades accuracy or causes complete outages [10], [14], [32]. Unlike in road traffic, these limitations are particularly acute on narrow sidewalks, where lane markings are absent, and the boundary between pedestrian and vehicle zones is ambiguous, making sub-decimeter accuracy a hard requirement for safe autonomous operation.

Ultra-wideband (UWB) technology has emerged as a promising complementary or alternative positioning solution, offering decimeter ranging accuracy for outdoor localization. UWB is based on ultra-short radio pulses transmitted across an exceptionally wide bandwidth of at least 500 MHz, enabling high temporal resolution and precise ranging. It achieves time-of-flight (ToF) measurements with theoretical ranging accuracy in the centimeter range under line-of-sight (LOS) conditions [1], [3], [7]. These properties result in UWB being inherently robust against multipath interference and narrowband noise, predominant error sources in conventional RF (Radio Frequency) positioning systems. The growing integration of UWB transceivers into commercial infrastructure further supports the vision of city-scale UWB-aided localization as a cost-effective complement to GNSS for future autonomous mobility systems [24].

This combination of ultra-wide bandwidth, centimeter-level ranging capability, and multipath robustness is directly relevant to the “Shared Guide Dog 4.0” developed at HAW Hamburg, a self-driving navigation device for blind and visually impaired individuals which requires sub-decimeter to centimeter outdoor positioning for use cases in urban scenarios [31]. The UWB system operates as a UWB localization setup consisting of fixed anchors and a mobile tag: anchors are deployed at known positions within the environment, typically mounted on existing urban infrastructure, while the tag is attached to the moving platform, which in this work corresponds to the *Shared Guide Dog 4.0*. The HAW Hamburg UWB beacon system for indoor [27], [28] and preliminary outdoor settings [31] has emerged from a series of student research works, confirming the suitability of the test environment and establishing the performance baseline from which this publication draws its experimental findings [32].

While UWB performance in indoor environments is well-established [9], [10], outdoor deployments introduce additional challenges stemming from environmental geometry and deployment constraints. First, the operating surface is often non-planar (i.e., sloped terrain), which introduces spatial variability in both user position and signal propagation conditions. Second, practical installation constraints prevent strict control over anchor geometry, including the inability to mount all anchors at the same physical height. In real urban deployments, anchors are typically attached to lampposts, building walls, or other fixed urban infrastructure, resulting in significant variations in elevation above ground level. Consequently, the anchor network forms a non-planar 3D geometry rather than an idealized planar configuration, raising a fundamental practical question: How does vertical heterogeneity in anchor placement affect 2D localization accuracy?

This question of vertical heterogeneity is addressed through a controlled outdoor experimental study using a custom UWB beacon system built at HAW Hamburg, based on a Qorvo DWM3000 module. We are investigating three anchor-height configurations within a defined 7 m × 10 m measurement field, evaluating both static tag positioning accuracy and dynamic trajectory performance under conditions representative of micromobility use cases [32].

The main contributions of this paper are:

(1) A systematic outdoor experimental study of UWB anchor vertical placement effects on 2D localization accuracy using production-grade UWB beacon DWM3000 hardware.

(2) Quantitative position statistics (σ_x, σ_y, $\Delta\bar{x}$, $\Delta\bar{y}$, σ_{2D}) and Horizontal Dilution of Precision (HDOP) analysis for three anchor-height configurations.

(3) Practical infrastructure design guidelines for UWB-based outdoor localization in GNSS-challenged urban environments.

II. Related Work

A. UWB Fundamentals and Standards

UWB localization rests on foundational signal theory established by Win and Scholtz [1], [2], who demonstrated that sub-nanosecond impulse-radio signals achieve exceptional temporal resolution for ranging. Dardari et al. [3] catalogued the primary error sources in multipath environments, while Shen and Win [25] derived information-theoretic limits showing that accuracy depends jointly on ranging quality and anchor geometry. Molisch [4] characterized UWB propagation channels relevant to outdoor deployments. The regulatory baseline is the IEEE 802.15.4z-2020 amendment [6], which standardized the enhanced UWB PHYs used by the DWM3000; Coppens et al. [24] and Alarifi et al. [9] review the changes of the IEEE UWB standards and the transceiver chipset development from 2007 to 2020. Gezici et al. [7] provide the foundational tutorial on UWB positioning methods covering time-of-arrival (ToA), time-difference-of-arrival (TDoA), and hybrid approaches.

B. UWB Localization at HAW Hamburg

A series of student research works at HAW Hamburg has progressively refined and extended the UWB beacon system developed at HAW Hamburg. Harnisch [27] conducted the first systematic performance characterization of the HAW UWB system, benchmarking accuracy and signal stability at distances from 2 m to 75 m. Koch [28] subsequently developed a two-stage UWB positioning system combining Kalman and particle filters with a reinforcement-learning-based correction, achieving up to 10 cm accuracy under indoor conditions. Koch [29] extended this work to automatic anchor-position calibration, significantly reducing infrastructure setup time and removing the need for manual survey measurements. Gleitzmann [30] demonstrated on-board UWB localization for a miniature watercraft platform (MS nHAWigatora) in laboratory and field conditions, achieving a median root-mean-square-error (RMSE) of 4.9 cm in controlled LOS environments and confirming the versatility of the HAW beacon design across mobile platform types. Obaid and Al-Aloush [31] conducted a preliminary outdoor investigation of the UWB system for the Shared Guide Dog 4.0, confirming a car park test site as suitable for outdoor UWB measurements with low building-induced interference. These works collectively form the research lineage from which the present study [32] is derived.

C. Indoor UWB Localization

Most published UWB localization research focuses on indoor environments. Ridolfi et al. [11]

demonstrated that UWB scalability in high-density deployments depends critically on anchor geometry. Tiemann et al. [12] applied UWB to UAV navigation in GNSS-denied indoor environments, achieving sub-decimeter accuracy with optimized anchor configurations. Zafari et al. [10] provided a comprehensive survey positioning UWB as the most accurate short-range radio technology. Marano et al. [13] addressed non-line-of-sight (NLOS) identification in UWB ranging, highlighting that ground-surface reflections are among the most significant error sources, a finding directly relevant to outdoor anchor-height studies. Patwari et al. [8] noted that non-uniform node heights introduce 3D geometric ambiguities degrading 2D estimation.

D. Outdoor UWB and Anchor-Height

Outdoor UWB research is comparatively sparse. Kristem et al. [14] experimentally measured ranging errors in a dense urban environment at antenna heights of 10 cm and 100 cm, finding that errors increase significantly when antennas are positioned closer to the ground, with NLOS errors exceeding 10 m when a building fully blocks the direct path. Lee et al. [15] provided the most comprehensive outdoor UWB dataset to date, sweeping antenna heights from 0.5 m to 2.0 m, and explicitly concluding that "ranging errors from ground reflections and Fresnel-zone attenuations depend on the antenna height." These errors "should be prevented in anchor deployment." The Wi-PoS outdoor platform [16] derived a ground-reflection path-loss model and achieved sub-5 cm accuracy at 50 to75 m outdoors.

As with UWB localization research in general, research on anchor placement geometry has also been studied primarily indoors. Kramařić et al. [17] evaluated UAV localization under varying indoor anchor configurations; Cho et al. [18] demonstrated that DOP does not always predict empirical error in compact UWB fields; Pan et al. [19] proposed genetic-algorithm-based anchor placement optimization; and Chen et al. [20] jointly optimized anchor placement and NLOS mitigation. Studies investigating DOP in UWB systems have shown that anchor-height affects z-axis DOP. Specifically, Feng et al. [21] and Yao et al. [22] reported this effect, although both studies were conducted indoors. Polonelli et al. [23] reported 33.2 % better ranging accuracy for the DW3000 (introduced in 2021) compared with the earlier-generation DW1000 (introduced in 2013) at short distances. Consistent with this generational shift, HAW Hamburg has likewise migrated from the widely adopted DW1000- to the DW3000-based UWB hardware.

E. Research Gap

To the best of the authors' knowledge, no prior study has experimentally isolated anchor vertical placement as a single variable in an outdoor UWB deployment using a ground-level mobile platform and current-generation Qorvo DWM3000 hardware, while evaluating accuracy via both 2D position statistics and DOP. This paper fills that gap, based on the experimental data of [32].

III. UWB System Description

A. Technology Fundamentals

UWB is defined by the Federal Communications Commission (FCC) as any signal occupying more than 500 MHz of bandwidth or exceeding 20 % of its center frequency. In practice, UWB operates in the frequency range between approximately 3.1 GHz and 10.6 GHz, well separated from narrowband technologies such as Bluetooth Low Energy (2.4 GHz) or Wi-Fi (2.4/5 GHz). UWB transmitters emit very short pulses (typical duration ≈ 100 ps to 2 ns) at low power spectral density (below −41.3 dBm/MHz), enabling precise ToA measurements.

UWB system uses the ToF technique to calculate the distance between two UWB nodes. The UWB tag transmits a frame at time $t1$, and the anchor receives it at $t2$. The drawback of this technique is that precise clock synchronization between all nodes is necessary.

The fundamental range (r) equation for ToF is:

$$r = c \cdot (t_2 - t_1) \quad (1)$$

$$r = c \cdot ToF \quad (2)$$

where c is the speed of light (299.8 × 10^6 m/s), t_1 is the transmission time, t_2 is the reception time, and ToF is calculated as $t_2 - t_1$.

The double-sided two-way ranging (DS-TWR) technique, used in this study [34], eliminates clock-synchronization requirements between anchor and tag [3]. DS-TWR is an extension of the two-way ranging (TWR) technique. In TWR (single-sided), a UWB node sends one message, waits for a reply, and calculates the round-trip time. The issue is that the anchor's clock and the tag's clock are never perfectly synchronized; even tiny differences in their oscillator frequencies (known as clock drift) introduce small timing errors which result in corresponding distance errors. DS-TWR mitigates this effect by performing the exchange twice, once measured from the anchor's clock and once from the tag's clock, and then combining both measurements mathematically such that the clock drift cancels out, as depicted in FIG. 1.

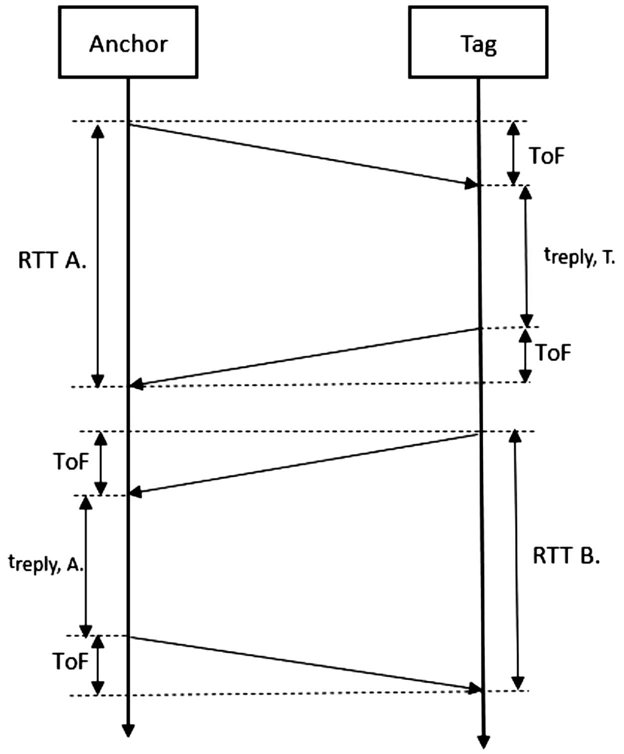

FIG. 1 DOUBLE-SIDED TWO-WAY RANGING (DS-TWR) TECHNIQUE [34]

$$RTT\ A. = 2 \cdot ToF + t_{reply,\ T.} \tag{3}$$

$$RTT\ B. = 2 \cdot ToF + t_{reply,\ A.} \tag{4}$$

$$RTT\ A. + RTT\ B. = 4 \cdot ToF + t_{reply,\ T.} + t_{reply,\ A.} \tag{5}$$

$$ToF_{DS-TWR} = \frac{RTT\ A. + RTT\ B. - t_{reply,\ T.} - t_{reply,\ A.}}{4} \tag{6}$$

$$r = c \cdot ToF_{DS-TWR} \tag{7}$$

Where RTT denotes the round-trip time, $RTT\ A.$ is the round-trip time A and $RTT\ B.$ is the round-trip time B, $t_{reply,\ T.}$ is the reply time of the tag, $t_{reply,\ A.}$ is reply time of the anchor.

B. Positioning via Trilateration

With at least three anchors at known positions, the tag location is estimated by trilateration: the intersection of spheres centered on each anchor with radii corresponding to the measured distances. The position is obtained by solving the nonlinear least-squares problem [35].

C. Hardware Platform — DWM3000 Beacon

The custom UWB beacon system, as depicted in FIG. 2, was designed and progressively refined at HAW Hamburg through a series of student works [27], [28], [29], [30], [31], [32], [33].

Each beacon integrates: (1) a Qorvo DWM3000 UWB transceiver (DW3110 chip, IEEE 802.15.4 [6], Channel 5, 6.4896 GHz, 499.2 MHz bandwidth) [5]; (2) an RP2040 dual-core 32-bit microcontroller (133 MHz) implementing DS-TWR and trilateration in firmware; and (3) an ESP32-C3 module for UART/Wi-Fi output. The enclosure meets IP67 weatherproofing with an integrated 2000 mAh Li-ion battery, enabling up to 40 Hz data acquisition [32]. Metallic fasteners were excluded from the antenna keep-out zone (10 mm clearance) to preserve the radiation pattern [5].

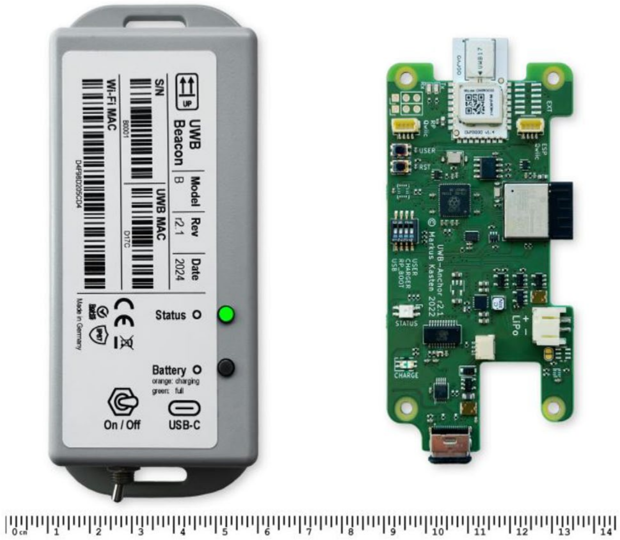

FIG. 2 UWB DWM3000 BEACON [29]

IV. EXPERIMENTAL METHODOLOGY

A. Test Site and General Setup

All experiments were conducted outdoors on the car parking lot at campus Berliner Tor, HAW Hamburg (GNSS coordinates 53.55703256° N, 10.02212560° E), a semi-open urban surface confirmed to exhibit low building-induced UWB interference in the preliminary study by Obaid and Al-Aloush [31].

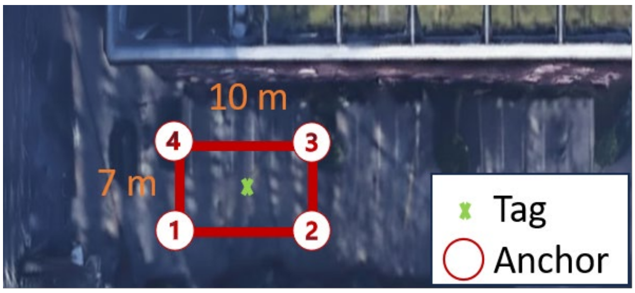

FIG. 3 TEST SITE CAR PARKING LOT BETWEEN BERLINER TOR 5 AND LÜBECKERTORDAMM 4 AT CAMPUS BERLINER TOR, HAW HAMBURG [SOURCE: GOOGLE EARTH]

The test field was a rectangle of 7 m (width) × 10 m (length), representative of a typical micromobility corridor or pedestrian pathway, as depicted in FIG. 3. Four UWB anchors and one tag were deployed. Anchors were mounted on 2 m PVC poles fixed to

0.7 m tripod stands (Hama LS-L200); all hardware in the antenna vicinity was plastic or taped to prevent metallic signal disruption [5]. A spirit level ensured beacon alignment at each position [32], as depicted in FIG. 4.

FIG. 4 SPIRIT LEVEL ALIGNMENT TO PREVENT UWB BEACON POSITIONED AT AN ANGLE [32]

B. Anchor-Height Configurations

The horizontal anchor footprint (7 m × 10 m rectangle) was held identical across all configurations, isolating the vertical placement effect from any horizontal geometric change [32]. The minimum anchor-height of 2.7 m was chosen to remain well above the first Fresnel-zone clearance, minimizing ground-reflection-induced ranging bias recommended by Kristem et al. [14] and Lee et al. [15]. Three sequential height Configurations were tested as described in TABLE I and depicted in FIG. 5.

Configuration	Height (m)	Description
A	2.7/2.7/2.7/2.7	All anchors have a uniform baseline
B	2.7/2.9/2.7/3.1	Two anchors raised (+20, +40 cm)
C	2.7/2.9/3.1/3.3	All anchors staggered (steps of +20 cm)

TABLE I ANCHOR-HEIGHT CONFIGURATIONS (A, B, AND C)

C. Reference Position and Measurement Procedure

The reference tag position was physically marked and measured with a tape measurement, giving two-dimensional (2D) coordinates (x_{ref}, y_{ref}) = (3.50 m, 5.00 m) relative to anchor-1 in FIG. 5. Ground-truth uncertainty is estimated at ±10 cm (tape alignment).

- Static Measurements: For each configuration (A to C), the tag was placed at the reference position, and approximately 4000+ samples were recorded over a 2-minute measurement series. The area was kept free of all people and moving objects (except the operator).

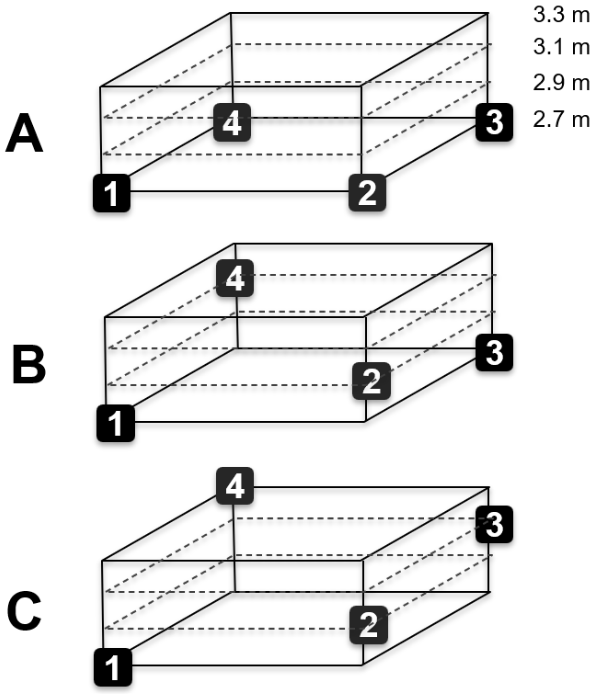

FIG. 5 ANCHOR-HEIGHT CONFIGURATIONS (A, B, AND C)

D. Evaluation Metrics

Position accuracy is evaluated using the mean position offsets, standard deviations, 2D positional scatter, and complemented by horizontal dilution of precision (HDOP) analysis [32].

$$\Delta\bar{x} = \bar{x} - x_{ref} \tag{8}$$

$$\Delta\bar{y} = \bar{y} - y_{ref} \tag{9}$$

$$\sigma_x = \sqrt{\frac{1}{N}\sum_i^N (x_i - \bar{x})^2} \tag{10}$$

$$\sigma_y = \sqrt{\frac{1}{N}\sum_i^N (y_i - \bar{y})^2} \tag{11}$$

$$\sigma_{2D} = \sqrt{\sigma_x^2 + \sigma_y^2} \tag{12}$$

Where $\Delta\bar{x}$ and $\Delta\bar{y}$ are the mean position offsets in the x- and y-axes, respectively; $\bar{x}$ and $\bar{y}$ are the mean values of measurement series in the x and y axes, respectively; x_{ref} and y_{ref} are the reference position coordinates in x- and y-axes, respectively; σ_x and σ_y are the standard deviations in the x- and y-axes, respectively; N is the number of measurements; x_i and y_i are the measured position values of the i-th measurement in the x- and y-axes, respectively; i = 1, 2, . . . , N is the sequence index of the measurements; and σ_{2D} is the 2D positional scatter.

DOP quantifies how strongly the geometric arrangement of anchors amplifies ranging errors into position errors. DOP is derived from the diagonal elements of the covariance matrix Q, where H is the linearized design matrix (13) of unit direction vectors between tag and anchors [32].

$$H = \begin{bmatrix} \frac{x-x_1}{r_1} & \frac{y-y_1}{r_1} \\ \frac{x-x_2}{r_2} & \frac{y-y_2}{r_2} \\ \vdots & \vdots \\ \frac{x-x_n}{r_n} & \frac{y-y_n}{r_n} \end{bmatrix} \tag{13}$$

Where x_i and y_i are known coordinates of n tracking anchors in x and y axes, respectively; r_i is true geometric 2D distance from tag to each anchor; and i = 1, 2,…, n represents the number of anchors.

$$r_i = \sqrt{(x - x_i)^2 + (y - y_i)^2} \tag{14}$$

$$Q = (H^T H)^{-1} \tag{15}$$

$$Q = \begin{bmatrix} q_{xx} & q_{xy} \\ q_{yx} & q_{yy} \end{bmatrix} \tag{16}$$

Where q_{xx} represents the geometric dilution variance scaling factor for the x-axis, q_{yy} represents the geometric dilution variance scaling factor for the y-axis. The horizontal dilution of precision (HDOP) is derived as:

$$HDOP = \sqrt{q_{xx} + q_{yy}} \tag{17}$$

The lower DOP indicates a favorable geometry. Standard classification: DOP ≤1 (Ideal), 1-2 (Excellent), 2-5 (Good), >5 (Poor). All HDOP values in this study lie in the “Excellent” range (1-2).

V. RESULT AND DISCUSSION

A. Static Position Statistics

TABLE II presents the static position statistics for all three anchor-height configurations [32]. The reference position of the tag is (x_{ref}, y_{ref}) = (3.50 m, 5.00 m).

Configuration	$\bar{x}$ (m)	$\bar{y}$ (m)	$\Delta\bar{x}$ (cm)	$\Delta\bar{y}$ (cm)	σ_x (cm)	σ_y (cm)	σ_{2D} (cm)
A	3.317	4.636	-18.3	-36.4	1.20	0.85	1.47
B	3.313	4.616	-18.7	-38.4	1.19	0.87	1.47
C	3.295	4.646	-20.5	-35.4	1.97	1.14	2.28

TABLE II STATIC POSITION STATISTICS VS ANCHOR-HEIGHT CONFIGURATIONS (x_{ref}=3.50 METER, y_{ref}=5.00 METER)

Several key observations emerge. First, the systematic positional offsets ($\Delta\bar{x}$ ≈ -18 to -21 cm; $\Delta\bar{y}$ ≈ -35 to -39 cm) are consistent across all Configurations, indicating a systematic bias independent of anchor-height. This bias is attributed to tape-based reference position measurement uncertainty (±10 cm [32]) combined with minor environmental reflections. Critically, since this offset is common to all configurations, it does not affect the comparison between anchor-height configurations.

Second, the positional scatter (σ_x , σ_y) is consistently low across all three configurations. Configurations A and B both achieve σ_x ≈ 1.2 cm and σ_y ≈ 0.9 cm, while Configuration C shows a modestly larger scatter of σ_x ≈ 2.0 cm and σ_y ≈ 1.1 cm. The combined two-dimensional scatter is σ_{2D} ≈ 1.5 cm for Configurations A and B, and σ_{2D} ≈ 2.3 cm for Configuration C, a moderate increase of roughly 55 % rather than a severe degradation, indicating that all three height configurations maintain good 2D positional stability.

The geometric explanation for this small increase is found in the structure of the direction-vector matrix H, which relates each anchor’s LOS direction to the tag with the resulting position error. Each anchor’s direction vector has a horizontal component (in the X-Y plane) and a vertical component (along the Z-axis). In the homogeneous configuration (Configuration A), all anchors are placed at the same height, so their direction vectors are nearly co-planar with a very limited vertical (Z-axis) component; ranging errors are therefore concentrated in, and distributed symmetrically, across the horizontal X-Y plane. In Configuration B, two anchors are raised by differing amounts from the baseline of 2.7 m: Δ of 0.2 m (2.9 m) and Δ of 0.4 m (3.1 m)) and alternated with the two baseline anchors (2.7 m) around the layout rather than grouped together; this interleaved arrangement adds a modest vertical (Z-axis) component to the geometry while keeping it evenly balanced across the four anchor positions so the low-scatter behavior of the baseline is preserved. In Configuration C, all four anchors are staggered across a wider 60 cm range. While the configuration remains height-symmetric in the sense that no single anchor stands out as an outlier, the larger spread of vertical (Z-axis) components shifts a small additional share of the ranging error from the vertical direction into the horizontal X-Y plane, producing the slightly larger but still well-controlled increase in horizontal scatter observed for this configuration.

B. Dilution of Precision Analysis

TABLE III presents the computed HDOP values for each configuration, derived from the design matrix H at the mean estimated tag position [32].

Configuration	HDOP
A	1.114
B	1.123
C	1.132

TABLE III HDOP VS ANCHOR-HEIGHT CONFIGURATIONS

HDOP remains nearly constant across all three configurations (1.114, 1.123, 1.132), confirming that the identical horizontal anchor footprint does not meaningfully change horizontal error amplification regardless of anchor-height variation. The marginal increase from Configuration A to Configuration C (ΔHDOP ≈ 0.018) is negligibly small and falls well within the “Excellent” classification (HDOP ≤ 2) throughout [36], indicating that the anchor-height configurations tested in this study do not compromise the horizontal geometric quality of the anchor layout.

C. Practical Infrastructure Guidelines

Synthesizing the static tag position measurements at 0.8 m height, 2D positional scatter and HDOP findings, the following design principles emerge for UWB anchor vertical placement when supporting 2D localization of a sidewalk-based mobile robot.

(1) Prefer uniform anchor-height (Configuration A) where infrastructure permits. This gives the lowest 2D positional scatter (σ_{2D} ≈ 1.5 cm) and the most predictable position estimate.

(2) Symmetric two-anchor-height (Configuration B) is an effective alternative when uniform anchor mounting is impractical. Real sidewalk anchor mounting points (posts, walls, railings) rarely match exactly. Configuration B shows that ±40 cm of alternating height incurs negligible degradation in 2D accuracy (σ_{2D} ≈1.5 cm) and only a marginal increase in HDOP.

(3) Fully staggered anchor-height (Configuration C) is usable but less accurate. A 60 cm height spread, e.g. from sloped terrain or mismatched mounts, raises 2D positional scatter to σ_{2D} ≈ 2.3 cm (≈ 55 % above baseline), acceptable for sidewalk robots.

(4) HDOP is nearly flat across all configurations (1.114-1.132), so it can’t flag Configuration C’s higher 2D positional scatter. Test-field validates actual 2D accuracy, not just HDOP, when anchor height varies substantially.

(5) Keep all anchors above 2.0 m to clear pedestrians, bicyclists, and robots, and avoid ground-reflection bias [14], [15].

(6) Results are static-only. Robot motion, curbs, slopes, and tag-height fluctuations during travel were not tested here and needed separate validation.

(7) The 7 m × 10 m test field is small relative to real sidewalk networks; results should be validated at larger scale before generalizing.

VI. CONCLUSION

This paper presented a static experimental study of the influence of UWB anchor vertical placement on 2D localization accuracy using Qorvo DWM3000-based beacons at HAW Hamburg. Three anchor-height configurations (A to C) were evaluated over a 7 m × 10 m outdoor test field, with the tag held at a fixed height of 0.8 m to simulate the sensor platform of a sidewalk-based mobile robot.

The results show that 2D positional scatter remains low and comparable for uniform (Configuration A) and moderately alternating anchor-height (Configuration B), with σ_{2D} ≈ 1.5 cm for both. A fully staggered height configuration (Configuration C, 60 cm spread) increases scatter moderately to σ_{2D} ≈ 2.3 cm, an increase of approximately 55% over the baseline. HDOP increases only marginally across all three configurations (1.114, 1.123, 1.132), remaining within the “Excellent” classification throughout, and does not by itself predict the scatter increase observed in Configuration C, indicating that vertical height diversity redistributes a small share of ranging error into the horizontal plane in a way that horizontal-footprint-based HDOP alone cannot capture.

These findings suggest that UWB anchors mounted at uniform or moderately varying heights are well-suited for 2D localization of mobile robots on sidewalks, while larger height disparities introduce a measurable but moderate accuracy cost. As the present results are based on static measurements over a comparatively small test field, they should be regarded as an initial geometric baseline. Future work should validate these findings under dynamic conditions with a moving robot platform, across larger-scale outdoor test sites, and account for tag-height variation caused by curbs, slopes, and uneven sidewalk surfaces.

VII. FUTURE WORK

Several extensions to this study would strengthen and broaden its conclusions. First, the present analysis is limited to static tag positions; future work should repeat these measurements with the tag mounted on a moving robot platform to assess whether the scatter trends observed here hold under dynamic conditions, including motion-induced multipath and Doppler effects. Second, the 7 m × 10 m test field used in this study is small relative to real sidewalk networks; validating the anchor-height effect at larger spatial scales and over longer anchor-to-tag distances would clarify whether the 55% scatter increase observed for Configuration C persists, grows, or diminishes with scale. Third, this study fixed the tag at a constant 0.8 m height; since a sidewalk robot crosses curbs, ramps, and uneven terrain, future measurements should quantify how small fluctuations in tag height – not just anchor-height – affect 2D accuracy. Fourth, the present test field was kept free of obstacles during measurement; future studies should introduce static obstructions (parked vehicles, street furniture, vegetation) and dynamic obstructions (pedestrians, cyclists, other moving robots) between anchors and tag to evaluate accuracy and HDOP under realistic NLOS and multipath conditions. Finally, extending the anchor-height range beyond the 60 cm tested here, and combining UWB with complementary sensing (e.g., IMU or wheel odometry), would help to establish more general design limits for outdoor UWB infrastructure supporting autonomous sidewalk navigation.

VIII. Acknowledgement

This work was supported by the German Federal Ministry of Research, Technology, and Space (BMFTR) under the "Safe Walker" project at HAW Hamburg. The authors gratefully acknowledge the contributions of Markus Kasten, Michel Harnisch, Sven Koch, Justus Gleitzmann, Mohammed Obaid, and Mohammad Al-Aloush, whose student research works at HAW Hamburg provided the experimental foundation and hardware platform on which this publication is based.

References

[1] M. Z. Win and R. A. Scholtz, "Impulse radio: How it works," IEEE Commun. Lett., vol. 2, no. 2, pp. 36–38, Feb. 1998. DOI: 10.1109/4234.660796

[2] M. Z. Win and R. A. Scholtz, "Ultra-wide bandwidth time-hopping spread-spectrum impulse radio for wireless multiple-access communications," IEEE Trans. Commun., vol. 48, no. 4, pp. 679–689, Apr. 2000. DOI: 10.1109/26.843135

[3] D. Dardari, A. Conti, U. J. Ferner, A. Giorgetti, and M. Z. Win, "Ranging with ultrawide bandwidth signals in multipath environments," Proc. IEEE, vol. 97, no. 2, pp. 404–426, 2009. DOI: 10.1109/JPROC.2008.2008846

[4] A. F. Molisch, "Ultra-wide-band propagation channels," Proc. IEEE, vol. 97, no. 2, pp. 353–371, 2009. DOI: 10.1109/JPROC.2008.2008836

[5] Qorvo Inc., "DWM3000 Series UWB Transceiver Datasheet," Rev. 2.3, May 2021. [Online]. Available: https://www.qorvo.com/products/p/DWM3000

[6] IEEE Std 802.15.4z-2020, "Enhanced Ultra Wideband (UWB) Physical Layers and Associated Ranging Techniques," IEEE, 2020. DOI: 10.1109/IEEESTD.2020.9179124

[7] S. Gezici, Z. Tian, G. B. Giannakis, H. Kobayashi, A. F. Molisch, H. V. Poor, and Z. Sahinoglu, "Localization via ultra-wideband radios," IEEE Signal Process. Mag., vol. 22, no. 4, pp. 70–84, 2005. DOI: 10.1109/MSP.2005.1458289

[8] N. Patwari, J. A. Ash, S. Kyperountas, A. O. Hero, R. L. Moses, and N. S. Correal, "Locating the nodes: cooperative localization in wireless sensor networks," IEEE Signal Process. Mag., vol. 22, no. 4, pp. 54–69, 2005.

[9] A. Alarifi, A. Al-Salman, M. Alsaleh, A. Alnafessah, S. Alhadhrami, M. A. Al-Ammar, and H. S. Al-Khalifa, "Ultra wideband indoor positioning technologies: analysis and recent advances," Sensors, vol. 16, no. 5, art. 707, 2016. DOI: 10.3390/s16050707

[10] F. Zafari, A. Gkelias, and K. K. Leung, "A survey of indoor localization systems and technologies," IEEE Commun. Surveys Tuts., vol. 21, no. 3, pp. 2568–2599, 2019. DOI: 10.1109/COMST.2019.2911558

[11] M. Ridolfi, A. Verfaillie, W. Van Stan, J. Hoebeke, I. Moerman, and E. De Poorter, "Analysis of the scalability of UWB indoor localization solutions for high user densities," Sensors, vol. 18, no. 6, p. 1875, 2018.

[12] J. Tiemann, F. Schweikowski, and C. Wietfeld, "Design of an UWB indoor-positioning system for UAV navigation in GNSS-denied environments," in Proc. IPIN 2015, pp. 1–7, IEEE, 2015.

[13] S. Marano, W. M. Gifford, H. Wymeersch, and M. Z. Win, "NLOS identification and mitigation for localization based on UWB experimental data," IEEE J. Sel. Areas Commun., vol. 28, no. 7, pp. 1026–1035, 2010. DOI: 10.1109/JSAC.2010.100907

[14] V. Kristem, S. Niranjayan, S. Sangodoyin, and A. F. Molisch, "Experimental determination of UWB ranging errors in an outdoor environment," in Proc. IEEE ICC, pp. 4838–4843, 2014. DOI: 10.1109/ICC.2014.6884086

[15] B.-H. Lee, J. Choi, S. Jeong, J. H. Choi, and K.-Y. Oh et al., "Comprehensive outdoor UWB dataset: static and dynamic measurements in LOS/NLOS environments," Scientific Data, vol. 12, art. 1532, 2025. DOI: 10.1038/s41597-025-05887-9

[16] B. Van Herbruggen, J. De Brouwer, and E. De Poorter, "Wi-PoS: a low-cost, open source ultra-wideband (UWB) hardware platform with long range sub-GHz backbone," Sensors, vol. 19, no. 7, art. 1548, 2019. DOI: 10.3390/s19071548

[17] L. Kramarić, M. Muštra, and T. Radišić, "The influence of ultra-wideband anchor placement on localization accuracy," Sensors, vol. 25, no. 16, art. 5115, 2025. DOI: 10.3390/s25165115

[18] J. Cho, S. Jeong, and B. Lee, "A study on anchor placement and 3D positioning algorithm for UWB in small sites," KSCE J. Civil Eng., vol. 28, pp. 4575–4587, 2024. DOI: 10.1007/s12205-024-2107-z

[19] H. Pan, X. Qi, M. Liu, and L. Liu, "An UWB-based indoor coplanar localization and anchor placement optimization method," Neural Comput. Appl., vol. 34, pp. 16845–16860, 2022. DOI: 10.1007/s00521-022-07329-8

[20] Y.-Y. Chen, S.-P. Huang, T.-W. Wu, W.-T. Tsai, C.-Y. Liou, and S.-G. Mao, "UWB system for indoor positioning and tracking with optimal

anchor location and adaptive NLOS mitigation," IEEE Trans. Veh. Technol., vol. 69, no. 9, pp. 9304–9314, 2020. DOI: 10.1109/TVT.2020.2972578

[21] G. Feng, C. Shen, C. Long, and F. Dong, "GDOP index in UWB indoor location system experiment," in Proc. IEEE SENSORS, 2015. DOI: 10.1109/ICSENS.2015.7370254

[22] L. Yao, L. Yao, and Y.-W. Wu, "Analysis and improvement of indoor positioning accuracy for UWB sensors," Sensors, vol. 21, no. 17, art. 5731, 2021. DOI: 10.3390/s21175731

[23] T. Polonelli, S. Schläpfer, and M. Magno, "Performance comparison between Decawave DW1000 and DW3000 in low-power double side ranging applications," in Proc. IEEE SAS, 2022. DOI: 10.1109/SAS54819.2022.9881375

[24] D. Coppens, A. Shahid, S. Lemey, B. Van Herbruggen, C. Marshall, and E. De Poorter, "An overview of UWB standards and organizations (IEEE 802.15.4, FiRa, Apple)," IEEE Access, vol. 10, pp. 70219–70241, 2022. DOI: 10.1109/ACCESS.2022.3187410

[25] Y. Shen and M. Z. Win, "Fundamental limits of wideband localization—Part I: A general framework," IEEE Trans. Inf. Theory, vol. 56, no. 10, pp. 4956–4980, 2010. DOI: 10.1109/TIT.2010.2060110

[26] B. Lu et al., "Assistive navigation using deep reinforcement learning guiding robot with UWB/voice beacons and semantic feedbacks for blind and visually impaired people," Front. Robot. AI, vol. 8, art. 654132, 2021. DOI: 10.3389/frobt.2021.654132

[27] M. Harnisch, "Bestimmung der Leistungsfähigkeit des Ultra-wideband-Systems der HAW Hamburg (Performance Characterization of the HAW Hamburg Ultra-Wideband System)," Studienarbeit, HAW Hamburg, Supervisors: Prof. Dr. H. Gärtner, P. Stahr, Aug. 2022.

[28] S. Koch, "Hochgenaue Positionsbestimmung mit Ultra-wideband und Reinforcement Learning (High-Accuracy Positioning with Ultra-Wideband and Reinforcement Learning)," B.Sc. Thesis, HAW Hamburg, Dept. Computer Science, Supervisor: Prof. Dr. S. Pareigis, Dec. 2021. [Online]. Available: https://autosys.informatik.haw-hamburg. de/papers/2021SvenKochBA.pdf

[29] S. Koch, "Automatische Kalibrierung von Ankerpositionen zur hochgenauen Positionsbestimmung mit Ultra-wideband (Automatic Calibration of Anchor Positions for High-Accuracy UWB Positioning)," M.Sc. Thesis, HAW Hamburg, Dept. Computer Science, Supervisor: Prof. Dr. S. Pareigis, Oct. 2025. [Online]. Available: https://autosys.informatik.haw-hamburg.de/papers/2025Koch.pdf

[30] J. Gleitzmann, "Experimentelle Untersuchung von On-Board-Lokalisierung auf einem Miniaturschiff mittels laufzeitbasierter Distanzmessung (Experimental Investigation of On-Board Localisation on a Miniature Ship Using Time-of-Flight Distance Measurement)," B.Sc. Thesis, HAW Hamburg, Faculty of Computer Science and Digital Society, Supervisor: Prof. Dr. T. Tiedemann, Mar. 2026.

[31] M. Obaid and M. Al-Aloush, "Experimentelle Untersuchung der Genauigkeitsgrenzen von Ultra-Wide-Band (UWB) für den Shared Guide Dog 4.0 (Experimental Investigation of UWB Accuracy Limits for the Shared Guide Dog 4.0)," Studienarbeit, HAW Hamburg, Supervisors: Prof. Dr. H. Gärtner, B. Patel, May 2025.

[32] M. Obaid, "Analyse von Genauigkeitsgrenzen und Optimierungspotenzialen beim Außeneinsatz von Ultrabreitband-Lokalisierungssystemen für Mikromobile (Analysis of Accuracy Limits and Optimization Potentials in the Outdoor Use of UWB Localization Systems for Micromobility Vehicles)," B.Sc. Thesis, HAW Hamburg, Faculty of Aviation and Automotive Systems, Supervisors: Prof. Dr. H. Gärtner, Prof. Dr. T. Tiedemann, Mar. 2026.

[33] M. Kasten, "Hardwareplattformen für autonome Straßenfahrzeuge im Maßstab 1:87 (Hardware Platforms for Autonomous Road Vehicles at 1:87 Scale)," B.Sc. Thesis, Hamburg University of Applied Sciences (HAW Hamburg), Faculty of Computer Science and Engineering, Dept. Computer Science, Supervisors: Prof. Dr. T. Tiedemann, Prof. Dr. S. Pareigis, Mar. 2021.

[34] D. Vukovic, "Lokalisierung und Genauigkeitsermittlung mittels Ultra Wideband (Localization and Accuracy Determination Using Ultra Wideband)," M.Sc. Thesis, Fachhochschule Vorarlberg, Dornbirn, Austria, Supervisors: Dr. A. Mitterbacher and Dr. M. Becker (Tridonic GmbH & Co KG), Aug. 2022.

[35] Z. Sahinoglu; S. Gezici; I. Güvenc: Ultra-wideband Positioning Systems: Theoretical Limits, Ranging Algorithms, and Protocols. Cambridge, UK: Cambridge University Press, 2008.

[36] S. Jyothirmaye, V. Satya Srinivas, B. Ramu, "Fast satellite selection techniques and DOPs for multi-GNSS positioning," in Proc. URSI AP-RASC 2019, New Delhi, India, Mar. 2019.